

# Numerical investigations on the resonance errors of multiscale discontinuous Galerkin methods for one-dimensional stationary Schrödinger equation

Bo Dong\* and Wei Wang<sup>†</sup>

## Abstract

In this paper, numerical experiments are carried out to investigate the impact of penalty parameters in the numerical traces on the resonance errors of high order multiscale discontinuous Galerkin (DG) methods [6, 7] for one-dimensional stationary Schrödinger equation. Previous work showed that penalty parameters were required to be positive in error analysis, but the methods with zero penalty parameters worked fine in numerical simulations on coarse meshes. In this work, by performing extensive numerical experiments, we discover that zero penalty parameters lead to resonance errors in the multiscale DG methods, and taking positive penalty parameters can effectively reduce resonance errors and make the matrix in the global linear system have better condition numbers.

**Key words:** discontinuous Galerkin method, multiscale method, resonance errors, one-dimensional Schrödinger equation

---

\*E-mail: bdong@umassd.edu. Department of Mathematics, University of Massachusetts Dartmouth, North Dartmouth, MA 02747.

<sup>†</sup>Corresponding author. E-mail: weiwang1@fiu.edu. Department of Mathematics & Statistics, Florida International University, Miami, FL, 33199.

# 1 Introduction

In this paper, we consider the following one-dimensional second-order equation

$$-\varepsilon^2 u'' - f(x)u = 0, \quad (1.1)$$

where  $\varepsilon > 0$  is a small parameter and  $f(x)$  is a real-valued smooth function. One example of this type of equation is the stationary Schrödinger equation in the modeling of quantum transport in nanoscale semiconductors [4, 14, 18].

Note that when  $f$  is positive, the solution to Eq. (1.1) is an oscillatory wave function and the wave length is at the scale of  $\varepsilon$ . For small  $\varepsilon$ , the solution is highly oscillatory and simulation using standard finite element or finite difference methods requires very fine meshes. In applications such as quantum transport, this equation needs to be repeatedly solved for different magnitudes of wave lengths and thus it is desirable to develop multiscale methods that can effectively approximate the wave solutions even on coarse meshes.

There have been ongoing efforts on developing multiscale finite element methods which perform better than their polynomial-based counterparts for equations with highly oscillatory solutions; see [1, 3, 11, 12, 10, 15, 16, 19, 20, 17, 21] and references therein. One of the popular ideas is to incorporate the information of small scale into non-polynomial basis functions so that oscillatory solutions can be captured on coarse meshes. In [2, 14], a second-order continuous finite element method based on WKB asymptotics was introduced and analyzed for solving the stationary Schrödinger equation. Similar multiscale methods in the discontinuous Galerkin (DG) framework were developed and analyzed for Eq. (1.1) in [18, 6]. In [7], the multiscale DG methods were extended to higher orders using two different approximate function spaces  $E^p$  and  $T^{2p-1}$  for  $p \geq 1$ . Thanks to the advantage of having no continuity constraints across element interfaces, the multiscale DG methods in [18, 7] have been extended to two dimensions in [13, 8, 9].

In the multiscale DG methods, the numerical traces have been written in the form of alternating fluxes with penalty terms. In [18], the third-order multiscale DG method using the  $E^2$  space with zero penalty parameters produced good results in simulation of Schrödinger equations in Resonant Tunneling Diode on coarse meshes. However, the error analysis in later work [6, 7, 8, 9] required that the penalty parameters be positive for proving the error estimates. Furthermore, numerical results in [6] showed that the

multiscale DG method using the space  $E^2$  has resonance errors around  $h \simeq \varepsilon$  when the penalty parameters are zero.

In this paper, we perform numerical experiments to further investigate how the values of penalty parameters affect the accuracy of general multiscale DG methods using  $E^p$  and  $T^{2p-1}$  spaces. Our numerical experiments indicate that if the exact solution lies in the approximation space, the approximate solutions from different choices of penalty parameter are all accurate up to rounding off errors. But in the general case when the exact solution is not in the approximation space, zero penalty parameter will result in noticeable resonance errors when  $h \simeq \varepsilon$ , while using positive penalty parameters will greatly reduce such resonance errors. This improvement is also observed in the condition number of the matrix in the resulting global linear system.

The rest of the paper is organized as follows. In section 2, we describe the multiscale DG methods and related error estimates in previous work. In section 3, we demonstrate numerical results for different choices of penalty parameters. The concluding remarks and future work are in Section 4.

## 2 Multiscale DG method

### 2.1 The DG formulation

We consider the equation (1.1) with open boundary conditions,

$$\begin{cases} -\varepsilon^2 u'' - f(x)u = 0, & x \in [a, b], \\ \varepsilon u'(a) + \mathbf{i}\sqrt{f_a}u(a) = 2\mathbf{i}\sqrt{f_a}, & \varepsilon u'(b) - \mathbf{i}\sqrt{f_b}u(b) = 0, \end{cases} \quad (2.1)$$

where  $f_a = f(a)$ ,  $f_b = f(b)$ , and  $\mathbf{i}$  is the imaginary unit.

By introducing an auxiliary variable  $q$ , we can rewrite the second-order equation in (2.1) into the mixed form

$$q - \varepsilon u' = 0, \quad -\varepsilon q' - f(x)u = 0, \quad (2.2a)$$

and the boundary conditions as

$$q(a) + \mathbf{i}\sqrt{f_a}u(a) = 2\mathbf{i}\sqrt{f_a}, \quad q(b) - \mathbf{i}\sqrt{f_b}u(b) = 0. \quad (2.2b)$$

To define multiscale DG methods for (2.2), we need to introduce some notation. Let  $a = x_{\frac{1}{2}} < x_{1+\frac{1}{2}} < \cdots < x_{N+\frac{1}{2}} = b$  be a partition of the

domain,  $\Omega_h := \{I_j = (x_{j-\frac{1}{2}}, x_{j+\frac{1}{2}}) : j = 1, \dots, N\}$  be the set of all elements, and  $h = \max_{j=1, \dots, N} (x_{j+\frac{1}{2}} - x_{j-\frac{1}{2}})$ .

We consider two families of multiscale finite element spaces that we introduced in [7]. The first approximate function space  $E^p$  is obtained by combining two exponential basis functions and polynomial basis. For any element  $I_j \in \Omega_h$ , we let

$$E^p|_{I_j} = \begin{cases} \text{span}\{e^{ik_j(x-x_j)}, e^{-ik_j(x-x_j)}\} & \text{if } p = 1, \\ \text{span}\{e^{\pm ik_j(x-x_j)}, 1, x, \dots, x^{p-2}\} & \text{if } p \geq 2, \end{cases}$$

where  $k_j = \sqrt{f(x_j)}/\varepsilon$  is the wave number, and  $x_j := \frac{1}{2}(x_{j-\frac{1}{2}} + x_{j+\frac{1}{2}})$  is the middle point of the element  $I_j$ . The second approximate function space  $T^{2p-1}$  contains exponential basis functions in pairs. On each element  $I_j \in \Omega_h$ ,

$$T^{2p-1}|_{I_j} = \text{span}\{e^{\pm ik_j(x-x_j)}, e^{\pm 2ik_j(x-x_j)}, \dots, e^{\pm pik_j(x-x_j)}\}$$

for any  $p \geq 1$ . Note that  $T^1 = E^1$ , and the basis functions of  $E^p$  and  $T^{2p-1}$  are globally discontinuous across element interfaces and contains the information on the small scale of the problem.

Our DG method for (2.2) is to seek approximate solutions  $u_h, q_h \in E^p$  or  $T^{2p-1}$  that satisfy the following weak formulation

$$\begin{aligned} \sum_{j=1}^N \int_{I_j} q_h \bar{w} dx + \varepsilon \sum_{j=1}^N \int_{I_j} u_h \bar{w}' dx - \varepsilon \sum_{j=1}^N \hat{u}_h \bar{w} \Big|_{x_{j-\frac{1}{2}}}^{x_{j+\frac{1}{2}}} &= 0, \\ \varepsilon \sum_{j=1}^N \int_{I_j} q_h \bar{v}' dx - \varepsilon \sum_{j=1}^N \hat{q}_h \bar{v} \Big|_{x_{j-\frac{1}{2}}}^{x_{j+\frac{1}{2}}} - \sum_{j=1}^N \int_{I_j} f u_h \bar{v} dx &= 0 \end{aligned} \quad (2.5)$$

for all test functions  $v_h, w_h \in E^p$  or  $T^{2p-1}$ , where  $\bar{w}$  is the complex conjugate of  $w$ .

The numerical traces  $\hat{u}_h$  and  $\hat{q}_h$  are defined in the same way as in [6, 7], that is, at the interior element interfaces,

$$\begin{aligned} \hat{u}_h(x_{j+\frac{1}{2}}) &= u_h^-(x_{j+\frac{1}{2}}) - \mathbf{i} \beta \llbracket q_h \rrbracket(x_{j+\frac{1}{2}}), \\ \hat{q}_h(x_{j+\frac{1}{2}}) &= q_h^+(x_{j+\frac{1}{2}}) + \mathbf{i} \alpha \llbracket u_h \rrbracket(x_{j+\frac{1}{2}}), \end{aligned} \quad (2.6)$$

where  $v^-(x_{j+\frac{1}{2}})$  and  $v^+(x_{j+\frac{1}{2}})$  are the left and right limits of  $v$  at  $x_{j+\frac{1}{2}}$ , respectively, and  $\llbracket v \rrbracket = v^- - v^+$  represents the jump across the interface.

At the two boundary points  $\{a, b\}$ ,

$$\begin{aligned}
\widehat{u}_h(a) &= (1 - \gamma)u_h(a) + \mathbf{i}\frac{\gamma}{\sqrt{f_a}}q_h(a) + 2\gamma, \\
\widehat{q}_h(a) &= \gamma q_h(a) - \mathbf{i}(1 - \gamma)\sqrt{f_a}u_h(a) + 2\mathbf{i}(1 - \gamma)\sqrt{f_a}, \\
\widehat{u}_h(b) &= (1 - \gamma)u_h(b) - \mathbf{i}\frac{\gamma}{\sqrt{f_b}}q_h(b), \\
\widehat{q}_h(b) &= \gamma q_h(b) + \mathbf{i}(1 - \gamma)\sqrt{f_b}u_h(b),
\end{aligned} \tag{2.7}$$

where  $\gamma$  can be any real constant in  $(0, 1)$ .

Note that when the penalty parameters  $\alpha$  and  $\beta$  in (2.6) are taken to be zero, the numerical traces at interior interfaces are alternating fluxes and the method reduces to MD-LDG method [5] with multiscale bases. Note also that the numerical traces in (2.7) satisfy

$$\widehat{q}_h(a) + \mathbf{i}\sqrt{f_a}\widehat{u}_h(a) = 2\mathbf{i}\sqrt{f_a}, \quad \widehat{q}_h(b) - \mathbf{i}\sqrt{f_b}\widehat{u}_h(b) = 0,$$

which coincide with the boundary conditions (2.2b) for the exact solution.

## 2.2 Error estimates in previous work

We have proved some error estimates for the multiscale DG method defined by (2.5)-(2.7) in our previous work. For ease of reading, we list them here. First, in [6] we proved the following error estimates for the multiscale DG method with the approximation space  $E^1$ .

**Theorem 2.1.** *Let  $u$  be the solution of the problem (2.1) and  $u_h \in E^1$  be the multiscale DG approximation defined by (2.5)-(2.7). Assume that  $\alpha$  and  $\beta$  are positive constants and  $0 < \gamma < 1$ . For any mesh size  $h > 0$ , we have*

$$\|u - u_h\| \leq C|f|_{1,\infty}\left(\frac{h^2}{\varepsilon} + \frac{h^3}{\varepsilon^2}\right)\|u\|,$$

where  $C$  is independent of  $\varepsilon$  and  $h$ .

This theorem shows that when  $f$  is constant, the approximate solution from the multiscale DG method will only have round-off errors. When  $f$  is not constant, the method has a second order convergence rate for any mesh size, including  $h \gtrsim \varepsilon$ .

For the multiscale DG method with higher order approximation spaces, we obtained the following error estimates in [7].

**Theorem 2.2.** *Suppose  $(u, q)$  is the exact solution of the problem (2.2),  $(u_h, q_h)$  is the solution of the multiscale DG method using  $E^p$  for  $p = 2$  or  $3$ , and  $(\tilde{u}_h, \tilde{q}_h)$  is the solution of the multiscale DG method using  $T^{2p-1}$  for  $p = 2$  or  $3$ . Assume that  $\alpha$  and  $\beta$  are positive constants and  $0 < \gamma < 1$ . When  $h$  is small enough, we have*

$$\|u - u_h\| \leq C h^{\min\{s+1, p+1\}} (\|u\|_{s+1} + \|q\|_{s+1}),$$

$$\|u - \tilde{u}_h\| \leq C h^{\min\{s+1, 2p\}} (\|u\|_{s+1} + \|q\|_{s+1}),$$

where  $C$  is independent of  $h$  but may depend on  $\varepsilon$ .

Note that error estimates in Theorem 2.2 are valid only if  $h$  is sufficiently small. There are no error estimates for higher order spaces on coarse meshes.

The proofs of Theorem 2.1 and Theorem 2.2 require the penalty parameters  $\alpha$  and  $\beta$  to be positive. Numerical simulations in [18] showed that the multiscale DG method using  $E^2$  with zero penalty parameters produced good results on coarse meshes. In this case, the global matrix in the linear system is banded and the variable  $q$  in Eq. (2.2a) can be solved locally, thus solving the linear system is more efficient than using positive penalty parameters. But in [6], we found that the multiscale DG method using  $E^2$  with zero penalty parameters has obvious resonance errors around  $h \simeq \varepsilon$ . Therefore, in the next section, we would like to numerically investigate how penalty parameters affect the errors of multiscale DG methods with  $E^p$  and  $T^{2p-1}$  spaces, especially in the region  $h \simeq \varepsilon$ .

### 3 Numerical results

In this section, we carry out numerical experiments for multiscale DG using high order spaces  $E^p$  and  $T^{2p-1}$ , in particular,  $E^1 (= T^1)$ ,  $E^2$ ,  $E^3$ ,  $T^3$  and  $T^5$ . We will test the methods with different penalty parameters, compare the behaviors of the approximate solutions, and inspect the occurrence of resonance errors. We will also investigate the relation between the resonance error and the condition number of the matrix resulting from the global linear system.

*Example 3.1.* In the first example, we consider the simple case of constant function  $f(x)$ . It is easy to see that in this case, the exact solution of (2.1) is in the high-order finite element spaces  $E^p$  and  $T^{2p-1}$ . Thus the multiscale

Table 3.1: Example 3.1:  $L^2$ -errors by multiscale DG with  $E^1$  for  $f(x) = 10$ .

$N$	$\varepsilon = 0.005$			$\varepsilon = 0.001$		
	$\alpha = \beta = 0$	$\alpha = \beta = 0.5$	$\alpha = \beta = 1$	$\alpha = \beta = 0$	$\alpha = \beta = 0.5$	$\alpha = \beta = 1$
10	4.00E-12	4.17E-12	4.62E-12	7.08E-11	7.63E-11	7.66E-11
20	3.95E-12	4.01E-12	4.36E-12	6.92E-11	7.19E-11	7.27E-11
40	4.53E-12	4.56E-12	4.78E-12	7.19E-11	7.26E-11	7.42E-11
80	4.58E-12	4.63E-12	4.61E-12	7.21E-11	7.34E-11	7.31E-11
160	2.62E-12	2.65E-12	2.65E-12	6.12E-11	6.15E-11	6.23E-11
200	6.71E-12	6.75E-12	6.77E-12	8.24E-11	8.23E-11	8.31E-11

DG method with these spaces can compute the solution exactly with only round-off errors. We choose  $f(x) = 10$  which is the same as in our previous work [6, 7]. In [7], we performed the experiments of the multiscale DG methods only with non-zero penalty parameters  $\alpha = \beta = 1$ . This time, we will compare the multiscale DG with three different magnitudes of penalty parameters  $\alpha = \beta = 0$ ,  $\alpha = \beta = 0.1$  and  $\alpha = \beta = 1$ . Note that  $\alpha = \beta = 0$  reduces the method to the standard MD-LDG method with multiscale bases.

The  $L^2$ -errors of the multiscale DG method with  $E^1$ ,  $E^2$ ,  $E^3$ ,  $T^3$  and  $T^5$  are shown in Tables 3.1-3.5 respectively. In each table, we compute the approximate solutions with three different magnitudes of penalty parameters  $\alpha = \beta = 0$ ,  $\alpha = \beta = 0.1$  and  $\alpha = \beta = 1$  for two different levels of  $\varepsilon$ ,  $\varepsilon = 0.005$  and  $\varepsilon = 0.001$ . These two values of  $\varepsilon$  are chosen because during the mesh refinement,  $h$  is changing from  $h > \varepsilon$ ,  $h \simeq \varepsilon$ , to  $h < \varepsilon$ . When  $h \simeq \varepsilon$ , the error may suddenly increase due to resonance.

For all the results in Tables 3.1-3.5, it is clear to see the round-off errors in double precision. For the same value of  $\varepsilon$ , the results are very similar for different penalty parameters. Because they all capture the solution exactly, there is no resonance errors in this example. We notice that when  $\varepsilon$  is smaller, the round-off error increases slightly. This is because we use more points in each element for the numerical integration of the exponential functions which accumulate round-off errors for smaller  $\varepsilon$ .

*Example 3.2.* Next, we consider the model equation (2.1) with a smooth positive function  $f(x) = \sin x + 2$  on  $[0, 1]$ . There is no simple explicit formula for the exact solution in this case and the solution is not in the finite element spaces. The reference solutions are computed by the MD-LDG method [5] using piecewise cubic polynomials on  $N = 500,000$  elements. We again test

Table 3.2: Example 3.1:  $L^2$ -errors by multiscale DG with  $E^2$  for  $f(x) = 10$ .

$N$	$\varepsilon = 0.005$			$\varepsilon = 0.001$		
	$\alpha = \beta = 0$	$\alpha = \beta = 0.5$	$\alpha = \beta = 1$	$\alpha = \beta = 0$	$\alpha = \beta = 0.5$	$\alpha = \beta = 1$
10	4.00E-12	4.18E-12	4.66E-12	7.08E-11	7.67E-11	7.67E-11
20	3.95E-12	4.01E-12	4.39E-12	6.93E-11	7.11E-11	7.31E-11
40	4.54E-12	4.56E-12	4.68E-12	7.19E-11	7.27E-11	7.45E-11
80	4.57E-12	4.61E-12	4.62E-12	7.21E-11	7.30E-11	7.42E-11
160	2.60E-12	2.61E-12	2.61E-12	6.14E-11	6.12E-11	6.19E-11
200	6.75E-12	6.75E-12	6.77E-12	8.22E-11	8.32E-11	8.22E-11

Table 3.3: Example 3.1:  $L^2$ -errors by multiscale DG with  $E^3$  for  $f(x) = 10$ .

$N$	$\varepsilon = 0.005$			$\varepsilon = 0.001$		
	$\alpha = \beta = 0$	$\alpha = \beta = 0.5$	$\alpha = \beta = 1$	$\alpha = \beta = 0$	$\alpha = \beta = 0.5$	$\alpha = \beta = 1$
10	6.49E-12	4.19E-12	4.66E-12	4.66E-09	7.74E-11	8.24E-09
20	3.95E-12	4.01E-12	4.15E-12	6.93E-11	1.52E-09	7.24E-11
40	4.54E-12	4.58E-12	4.68E-12	7.19E-11	7.28E-11	7.44E-11
80	4.56E-12	4.58E-12	4.60E-12	7.20E-11	7.28E-11	7.29E-11
160	2.61E-12	2.62E-12	2.61E-12	6.10E-11	6.18E-11	6.09E-11
200	6.71E-12	6.72E-12	6.77E-12	8.22E-11	8.27E-11	8.27E-11

Table 3.4: Example 3.1:  $L^2$ -errors by multiscale DG with  $T^3$  for  $f(x) = 10$ .

$N$	$\varepsilon = 0.005$			$\varepsilon = 0.001$		
	$\alpha = \beta = 0$	$\alpha = \beta = 0.5$	$\alpha = \beta = 1$	$\alpha = \beta = 0$	$\alpha = \beta = 0.5$	$\alpha = \beta = 1$
10	4.01E-12	4.17E-12	4.66E-12	7.09E-11	7.62E-11	7.56E-11
20	3.95E-12	4.01E-12	4.37E-12	6.98E-11	7.19E-11	7.24E-11
40	4.55E-12	4.56E-12	4.76E-12	7.19E-11	7.59E-11	7.44E-11
80	4.83E-12	4.68E-12	4.62E-12	7.24E-11	7.36E-11	7.75E-11
160	2.62E-12	2.64E-12	2.65E-12	6.13E-11	6.16E-11	6.74E-11
200	6.72E-12	6.72E-12	6.37E-12	8.22E-11	8.23E-11	8.35E-11



Table 3.5: Example 3.1:  $L^2$ -errors by multiscale DG with  $T^5$  for  $f(x) = 10$ .

$N$	$\varepsilon = 0.005$			$\varepsilon = 0.001$		
	$\alpha = \beta = 0$	$\alpha = \beta = 0.5$	$\alpha = \beta = 1$	$\alpha = \beta = 0$	$\alpha = \beta = 0.5$	$\alpha = \beta = 1$
10	4.01E-12	4.19E-12	4.62E-12	7.57E-11	8.66E-11	8.58E-11
20	3.93E-12	4.01E-12	4.39E-12	6.98E-11	7.20E-11	7.05E-11
40	4.55E-12	4.58E-12	4.75E-12	7.18E-11	7.39E-11	7.39E-11
80	4.51E-12	4.58E-12	4.65E-12	7.23E-11	7.37E-11	7.53E-11
160	2.62E-12	2.62E-12	2.65E-12	6.14E-11	6.16E-11	6.82E-11
200	6.72E-12	6.72E-12	6.77E-12	8.31E-11	8.30E-11	8.33E-11

three different magnitudes of penalty parameters  $\alpha = \beta = 0$ ,  $\alpha = \beta = 0.1$  and  $\alpha = \beta = 1$  for five different order spaces  $E^1(= T^1)$ ,  $E^2$ ,  $E^3$ ,  $T^3$  and  $T^5$ . We consider two values of  $\varepsilon$ :  $\varepsilon = 0.005$  and  $0.001$ . The mesh is refined from  $N = 5$  to  $N = 640$ .

Fig. 3.1 shows the log-log plot of  $L^2$ -errors of  $u$  versus the number of elements  $N$  on the left and the corresponding condition numbers versus  $N$  on the right for the multiscale DG  $E^1$  with  $\varepsilon = 0.005$ . In each figure, we compare the results from three different magnitudes of penalty parameters  $\alpha = \beta = 0$ ,  $\alpha = \beta = 0.1$  and  $\alpha = \beta = 1$ . We can see the multiscale DG  $E^1$  with  $\alpha = \beta = 0$  (in red) has resonance errors around  $N = 30$ . Away from the resonance location, the method shows a second order of convergence. The multiscale DG  $E^1$  with positive parameters  $\alpha = \beta = 0.1$  (green) and  $\alpha = \beta = 1$  (blue) do not show any resonance errors and both of them have the second order of convergence for all  $N$ , which is consistent with Theorem 2.1. Thus, we can see that positive penalty parameters significantly help reduce the resonance errors.

Next, we look at the plot of condition numbers on the right of Figure 3.1. We see a big spike appearing at the same resonance location  $N = 30$  for the multiscale DG  $E^1$  with  $\alpha = \beta = 0$ . But the condition number plots for  $\alpha = \beta = 0.1$  and  $\alpha = \beta = 1$  are slowly increasing without spikes. This suggests that resonance errors are related to the suddenly increased condition numbers. We also observe that the method using  $\alpha = \beta = 0.1$  behaves slightly better than  $\alpha = \beta = 1$  for having smaller errors and condition numbers.

We plot figures for multiscale DG  $E^2$  in Fig. 3.2 with  $\varepsilon = 0.005$ . We can see the method with  $\alpha = \beta = 0$  has resonance errors around  $N = 30$  and

$N = 45$  on the left of Fig. 3.2. At the same locations, condition number plot has spikes too (see Fig. 3.2 right). The multiscale DG  $E^2$  with  $\alpha = \beta = 0.1$  and  $\alpha = \beta = 1$  do not have resonance errors. We observe a second order convergence when  $h \gtrsim \varepsilon$ . The approximate solutions show an optimal third order convergence when  $h \lesssim \varepsilon$ , which is consistent with Theorem 2.2. For zero penalty parameters, the method has similar convergence orders in the regions away from the resonance location.

We can see similar phenomenon for multiscale DG  $E^3$  in Fig. 3.3 with  $\varepsilon = 0.005$ . The method with  $\alpha = \beta = 0$  has resonance errors around  $N = 25$  and condition number has a big spike at the same location too. Away from the resonance area, we observe that all three choices of penalty parameters lead to a second order convergence when  $h \gtrsim \varepsilon$  and an optimal fourth order convergence when  $h \lesssim \varepsilon$ .

For the other fourth order space  $T^3$ , the resonance errors occur around  $N = 40$  in Fig. 3.4. It shows a similar second order convergence when  $h \gtrsim \varepsilon$  and optimal fourth order convergence when  $h \lesssim \varepsilon$ .

In Fig. 3.5, the multiscale DG  $T^5$  with  $\alpha = \beta = 0$  has two resonance errors regions around  $N = 40$  and  $N = 70$ . The condition number has spikes at the same locations. Away from the resonance area, we observe that the multiscale DG  $T^5$  with all three choice of penalty parameters has a second order convergence when  $h \gtrsim \varepsilon$  and an optimal sixth order convergence when  $h \lesssim \varepsilon$ .

When  $\varepsilon$  reduces to 0.001, which is  $1/5$  of 0.005, we expect the resonance location  $N$  to be 5 times of that for  $\varepsilon = 0.005$ . As we see in the error plot in Fig. 3.6, the multiscale DG  $E^1$  has resonance around  $N = 140$ , which is about 5 times of previous  $N = 30$  in Fig. 3.1. The condition numbers show spikes at the same locations. We can see similar phenomenon for multiscale DG with  $E^2$ ,  $E^3$ ,  $T^3$  and  $T^5$  as well; see Fig. 3.7-3.10.

## 4 Concluding remarks

In this paper, we carry out numerical experiments and have the following findings:

1. We observe resonance errors in multiscale DG with  $\alpha = \beta = 0$  for all five different spaces  $E^1(= T^1)$ ,  $E^2$ ,  $E^3$ ,  $T^3$  and  $T^5$ . The multiscale DG with positive penalty parameters have almost no resonance errors. Thus taking positive penalty parameters significantly helps reduce the resonance errors.

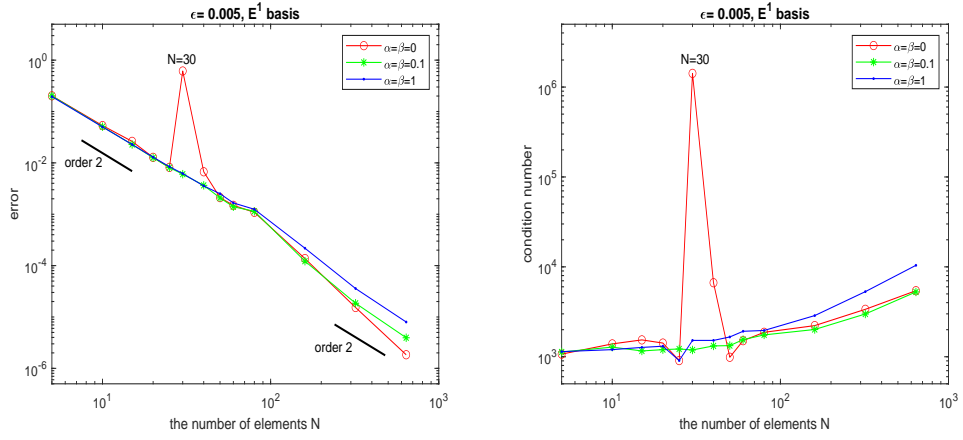


Figure 3.1: Example 3.2: Numerical results by multiscale DG  $E^1$  for  $\varepsilon = 5 \times 10^{-3}$ . Left:  $L^2$ -errors of  $u$ . Right: condition numbers.

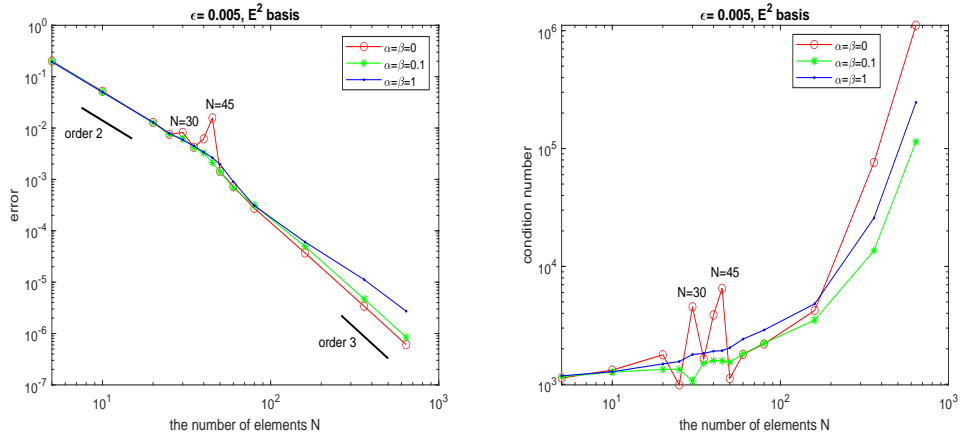


Figure 3.2: Example 3.2: Numerical results by multiscale DG  $E^2$  for  $\varepsilon = 5 \times 10^{-3}$ . Left:  $L^2$ -errors of  $u$ . Right: condition numbers.

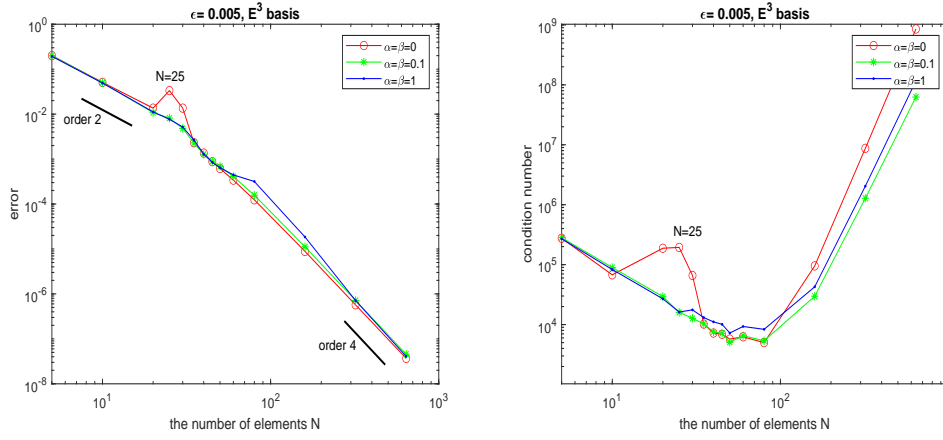


Figure 3.3: Example 3.2: Numerical results by multiscale DG  $E^3$  for  $\varepsilon = 5 \times 10^{-3}$ . Left:  $L^2$ -errors of  $u$ . Right: condition numbers.

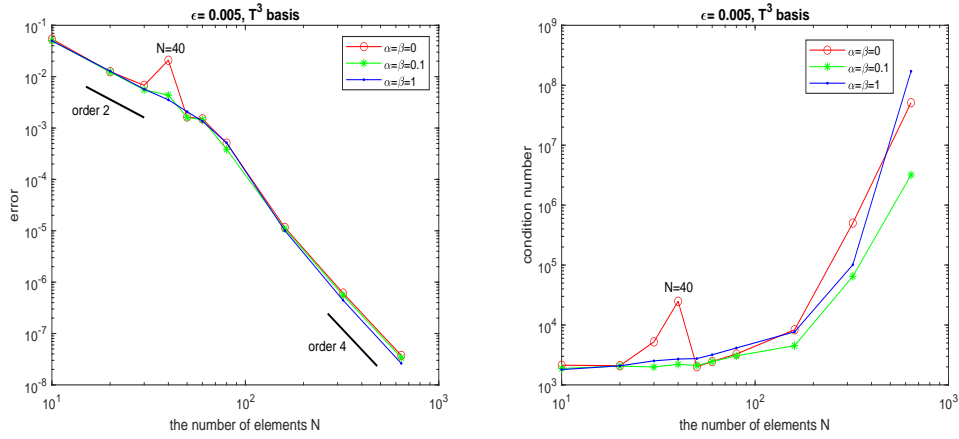


Figure 3.4: Example 3.2: Numerical results by multiscale DG  $T^3$  for  $\varepsilon = 5 \times 10^{-3}$ . Left:  $L^2$ -errors of  $u$ . Right: condition numbers.

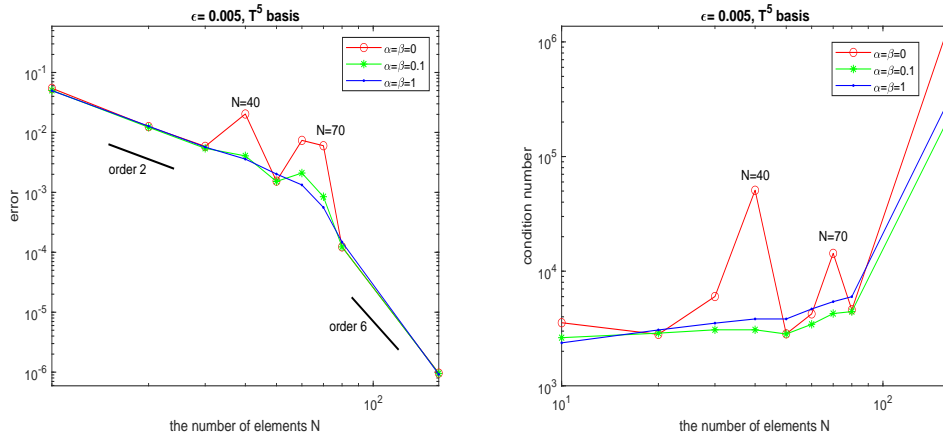


Figure 3.5: Example 3.2: Numerical results by multiscale DG  $T^5$  for  $\varepsilon = 5 \times 10^{-3}$ . Left:  $L^2$ -errors of  $u$ . Right: condition numbers.

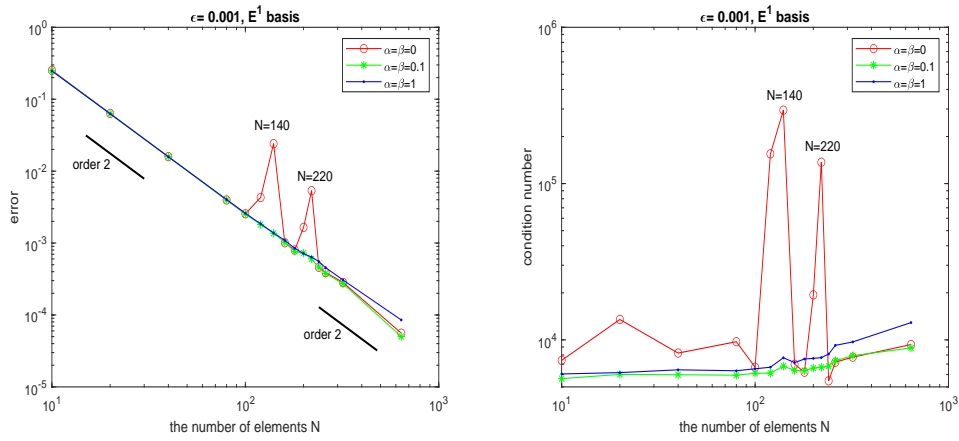


Figure 3.6: Example 3.2: Numerical results by multiscale DG  $E^1$  for  $\varepsilon = 1 \times 10^{-3}$ . Left:  $L^2$ -errors of  $u$ . Right: condition numbers.

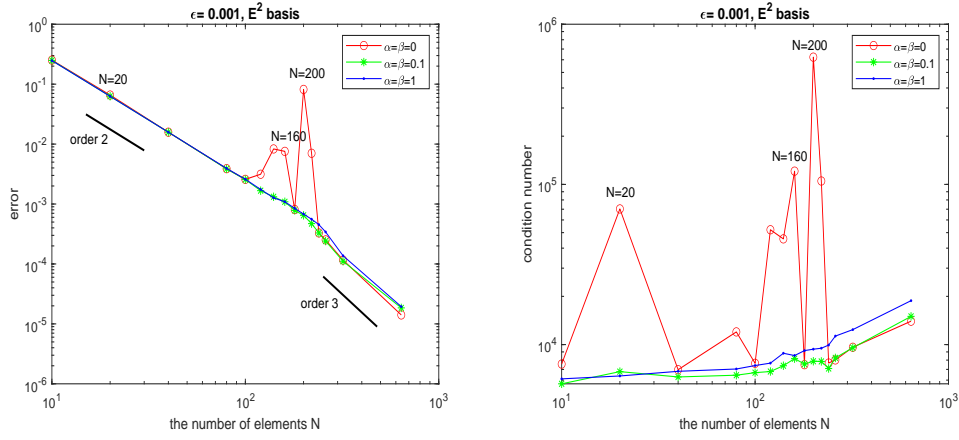


Figure 3.7: Example 3.2: Numerical results by multiscale DG  $E^2$  for  $\varepsilon = 1 \times 10^{-3}$ . Left:  $L^2$ -errors of  $u$ . Right: condition numbers.

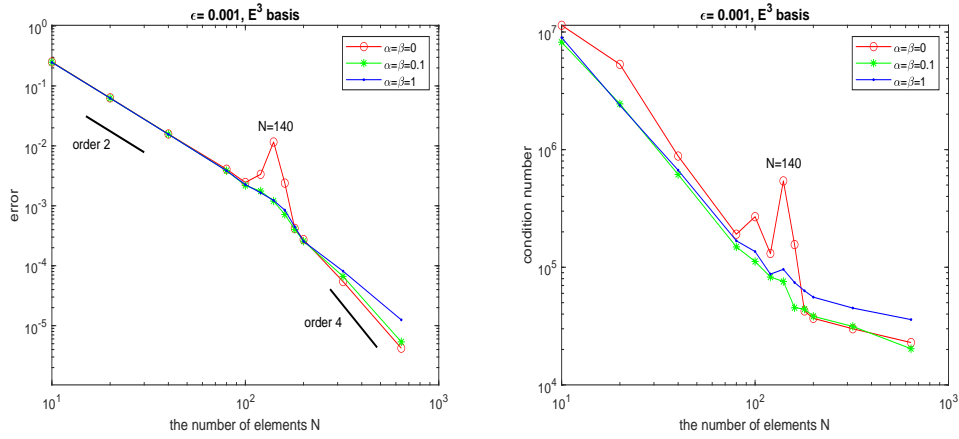


Figure 3.8: Example 3.2: Numerical results by multiscale DG  $E^3$  for  $\varepsilon = 1 \times 10^{-3}$ . Left:  $L^2$ -errors of  $u$ . Right: condition numbers.

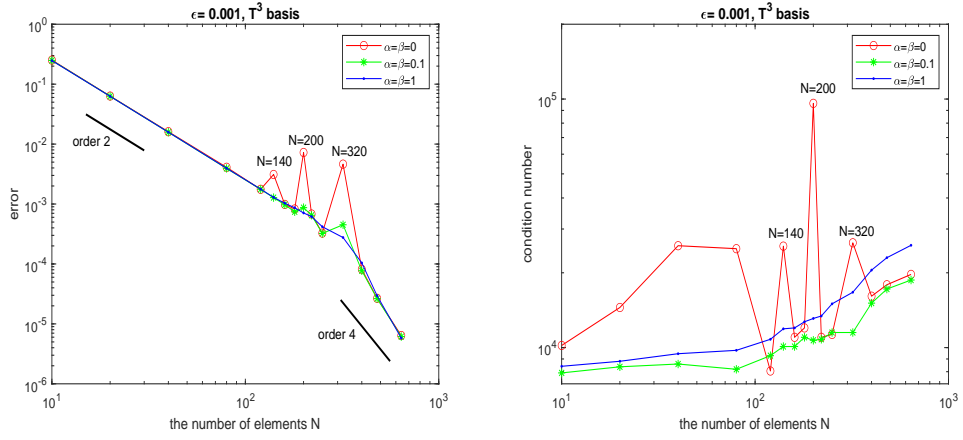


Figure 3.9: Example 3.2: Numerical results by multiscale DG  $T^3$  for  $\varepsilon = 1 \times 10^{-3}$ . Left:  $L^2$ -errors of  $u$ . Right: condition numbers.

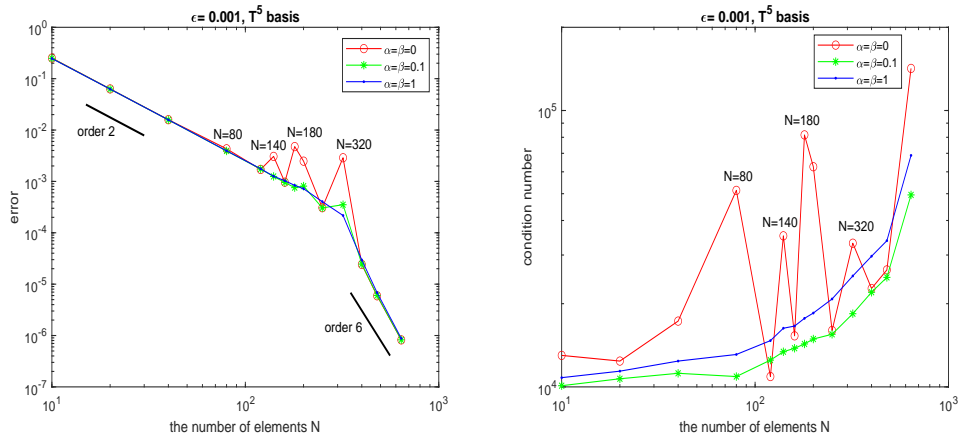


Figure 3.10: Example 3.2: Numerical results by multiscale DG  $T^5$  for  $\varepsilon = 1 \times 10^{-3}$ . Left:  $L^2$ -errors of  $u$ . Right: condition numbers.

2. In general, the resonance errors occur around  $h \simeq \varepsilon$ . For different function spaces  $E^p$  or  $T^{2p-1}$ , the resonance errors may occur at different locations. Some may be around one mesh point, some may be in a small region. But the graph of corresponding condition numbers has spikes at the same locations.

3. Multiscale DG methods with positive penalty parameters show second order convergence when  $h \gtrsim \varepsilon$  and optimal order convergence when  $h \lesssim \varepsilon$ . Multiscale DG methods with  $\alpha = \beta = 0$  behave similarly when the mesh size  $h$  is away from the resonance location  $h \simeq \varepsilon$ .

In the future work, we would like to investigate the resonance errors of multiscale discontinuous Galerkin methods for two-dimensional Schrödinger equation in [8, 9].

## 5 Acknowledgments

The authors consent to comply with all the Publication Ethical Standards. The research of the first author is supported by National Science Foundation grant DMS-1818998.

## 6 Conflict of interest

The authors declare that they have no conflict of interest.

## References

- [1] J. Aarnes and B.-O. Heimsund, *Multiscale discontinuous Galerkin methods for elliptic problems with multiple scales*, Multiscale methods in science and engineering 1–20, Lect. Notes Comput. Sci. Eng., 44. Springer, Berlin, 2005.
- [2] A. Arnold, N Ben Abdallah and C. Negulescu, WKB-based schemes for the oscillatory 1D Schrödinger equation in the semiclassical limit, SIAM J. Numer. Anal., 49, 2011, 1436–1460.
- [3] N. Ben Abdallah, M. Mouis and C. Negulescu, *An accelerated algorithm for 2D simulations of the quantum ballistic transport in nanoscale MOS-FETs*, J. Comput. Phys., **225**, 2007, 74–99.



- [4] N. Ben Abdallah and O. Pinaud, *Multiscale simulation of transport in an open quantum system: Resonances and WKB interpolation*, J. Comput. Phys., **213**, 2006, 288–310.
- [5] B. Cockburn and B. Dong, *An analysis of the minimal dissipation local discontinuous Galerkin method for convection-diffusion problems*, J. Sci. Comput., **32**, 2007, 233–262.
- [6] B. Dong, C.-W. Shu and W. Wang, *A new multiscale discontinuous Galerkin method for the one-dimensional stationary Schrodinger equation*, J. Sci. Comput., **66**, 2016, 321–345.
- [7] B. Dong and W. Wang, *High-order multiscale discontinuous Galerkin methods for the one-dimensional stationary Schrodinger equation*, J. Comput. and Applied Mathematics, **380**, 2020, 1–11.
- [8] B. Dong and W. Wang, *A high-order multiscale discontinuous Galerkin method for two-dimensional Schrödinger equation in quantum transport*, J. Comput. and Applied Mathematics, 2022, in press, <https://doi.org/10.1016/j.cam.2022.114701>.
- [9] B. Dong and W. Wang, *A new multiscale discontinuous Galerkin method for a class of second-order equations with oscillatory solutions in two-dimensional space*, Spectral and High Order Methods for Partial Differential Equations ICOSAHOM 2020+1, Lecture Notes in Computational Science and Engineering, Springer Nature Switzerland AG, accepted.
- [10] Y.R. Efendiev and T.Y. Hou, *Multiscale finite element methods: theory and applications*, Springer, New York, 2009.
- [11] G. Gabard, *Discontinuous Galerkin methods with plane waves for time-harmonic problems*, J. Comput. Phys., **225**, 2007, 1961–1984.
- [12] C. Gittelsohn, R. Hiptmair, and I. Perugia, *Plane wave discontinuous Galerkin methods: Analysis of the h-version*, ESAIM: M2AN Math. Model. Numer. Anal., **43**, 2009, 297–331.
- [13] L. Guo and Y. Xu, *Local Discontinuous Galerkin Methods for the 2D Simulation of Quantum Transport Phenomena on Quantum Directional Coupler*, Commun. Comput. Phys., **15**, 2014, 1012–1028.

- [14] C. Negulescu, *Numerical analysis of a multiscale finite element scheme for the resolution of the stationary Schrödinger equation*, Numer. Math., **108**, 2008, 625–652.
- [15] C. Negulescu, N. Ben Abdallah, E. Polizzi and M. Mouis, *Simulation schemes in 2D nanoscale MOSFETs: A WKB based method*, J. Comput. Electron., **3**, 2004, 397–400.
- [16] E. Polizzi and N. Ben Abdallah, *Subband decomposition approach for the simulation of quantum electron transport in nanostructures*, J. Comput. Phys., **202**, 2005, 150–180.
- [17] W. Wang, J. Guzmán and C.-W. Shu, *The multiscale discontinuous Galerkin method for solving a class of second order elliptic problems with rough coefficients*, Int. J. Numer. Anal. Model, **8**, 2011, 28–47.
- [18] W. Wang and C.-W. Shu, *The WKB local discontinuous Galerkin method for the simulation of Schrödinger equation in a resonant tunneling diode*, J. Sci. Comput., **40**, 2009, 360–374.
- [19] L. Yuan and C.-W. Shu, *Discontinuous Galerkin method based on non-polynomial approximation spaces*, J. Comput. Phys., **218**, 2006, 295–323.
- [20] L. Yuan and C.-W. Shu, *Discontinuous Galerkin method for a class of elliptic multi-scale problems*, Int. J. Numer. Meth. Fluids, **56**, 2008, 1017–1032.
- [21] Y. Zhang, W. Wang, J. Guzmán and C.-W. Shu, *Multi-scale discontinuous Galerkin method for solving elliptic problems with curvilinear unidirectional rough coefficients*, J. Sci. Comput., **61**, 2014, 42–60.